Results in Chemistry 4 (2022) 100537

Contents lists available at ScienceDirect

Results in Chemistry

journal homepage: www.sciencedirect.com/journal/results-in-chemistry

Efficient photocatalytic degradation of eosin blue dye and antibacterial study using nanostructured zinc oxide and nickel modified zinc oxide

Mansi H. Magar [a,b], Vishnu A. Adole [b,*], Ravindra H. Waghchaure [c], Thansing B. Pawar [b]

[a] Department of Chemistry, MVP's GMD Arts BW Commerce and Science College, Sinnar, Taluka-Sinnar, District – Nashik-422103, India[1]
[b] Research Centre in Chemistry, MGV's Loknete Vyankatrao Hiray Arts, Science and Commerce College Panchavati, Nashik 422003, India[1]
[c] Department of Chemistry, Mahant Jamanadas Maharaj Arts, Commerce and Science College, Karanjali, Taluka-Peth, District – Nashik-422 208, India[1]

ARTICLE INFO

Keywords:
Ni/ZnO
EB dye
Photocatalysis
Antibacterial screening

ABSTRACT

This article describes the fabrication of ZnO and 5% Ni^{2+} modified ZnO nanocatalyst (Ni/ZnO) for the photocatalytic degradation of eosin blue (EB) dye. To demonstrate the successful formation of nanocatalyst and study the structural and morphological aspects, as well as the chemical compositions, we employed X-ray diffraction (XRD), scanning electron microscopy (SEM), and energy dispersive spectroscopy (EDS) techniques. The optical band gap was investigated using Ultraviolet–visible (UV–Vis) spectroscopy, whereas the Zn-O band was revealed using Fourier transform infrared (FTIR) spectroscopy. To illustrate the optimized photocatalytic conditions for the degradation of EB dye, the parameters like initial EB dye concentration, catalyst loading, pH effect, and contact time were investigated. When compared to undoped ZnO and other reported nanocatalyst, the Ni/ZnO nanocatalyst displayed significantly better photocatalytic performance in the photocatalytic degradation of EB dye. With 0.8 g/L catalyst loading, 110 min contact period, and 8.0 pH, the photocatalytic efficiency was higher. Under optimized photocatalytic conditions, the results suggested that a Ni/ZnO nanocatalyst could be a potential nanomaterial for developing an enhanced doped nanocatalyst for EB removal. To confirm the presence of reactive oxygen species during photocatalysis, a radical scavenging experiment was performed using benzoquinone and isopropyl alcohol scavengers. The reusability of the produced nanocatalyst for four cycles confirms its stability and efficiency over multiple cycles. Furthermore, the Ni/ZnO was found to have significant antibacterial action against *Staphylococcus aureus*.

1. Introduction

Nanotechnology has recently been an important topic for investigators to build innovative nanoparticle-based devices with interesting applications in material science [1,2]. Drug delivery systems [3], biomedical [4,5], catalysis [6], imaging [7], sensing [8] and other industries could benefit from these nanosized materials. Nanomaterials, in particular, are attractive materials for catalysis applications because they have huge surface areas and better optical/electronic characteristics than bulk materials [9,10]. The most pressing worldwide issue of the twenty-first century is the provision of and assurance of safe water for the entire ecosystem. Water contamination is primarily caused by the rapid rise of industry [11]. Dyes are an organic compound that is widely utilised in the textile, printing, and food industries [12–14]. Dye effluents have a negative impact on the environment, and the majority of them are extremely toxic and non-biodegradable [15]. Eosin blue (EB) is a highly poisonous and carcinogenic phenothiazine pigment used in the dyeing of materials [16]. Traditional methods for removing these extremely dangerous synthetics, such as adsorption and ozonation, have been tried; however, due to various restrictions, these foreign chemicals cannot be removed from waste water [17,18]. Decontamination methods include adsorption [19], biological degradation [20], membrane filtration [21], photocatalytic degradation [22], reverse osmosis [23], nanofiltrations [24], oxidation [25], and others. Photocatalysis has a number of advantages above all other catalytic techniques. Reaction conditions like as solar energy, room temperature, and normal atmospheric pressure are common and easy to get. In addition, no harmful substances or by-products are produced throughout the breakdown process. Photocatalytic technology has become a diverse, intuitive, and cost-effective technology because the photocatalyst is at its

* Corresponding author.
E-mail address: vishnuadole86@gmail.com (V.A. Adole).
[1] Affiliated to Savitribai Phule Pune University, Pune (MH), India.

https://doi.org/10.1016/j.rechem.2022.100537
Received 18 July 2022; Accepted 20 September 2022
Available online 21 September 2022

core and numerous materials can act as a photocatalyst [19,22,26–30].

Metals are employed in waste water treatment processes to eliminate hazardous pollutants without releasing secondary contaminants, which protects the environment. For semiconductor-based photocatalysis, solar irradiation is the best natural energy source [31]. Solar irradiation, on the other hand, can only be used optimally for photocatalysis if a solar-irradiation-driven photocatalytic system is built. Many semiconducting metal oxides have been used in heterogeneous photocatalysis, including TiO_2, WO_3, Bi_2O_3, CuO, SnO_2, ZnO, and others [32–37]. Because of their greater band gap, the bulk of these semiconductors require UV irradiation for photocatalysis. When a wide-band-gap photocatalyst is exposed to UV irradiation with an energy equivalent to or greater than its band-gap energy, electron–hole pairs occur.

Due to its unique properties, such as a direct and broad band gap (3.37 eV) near-UV spectral area, increased oxidation ability, superior photocatalytic function, and a significant free-exciton binding energy, ZnO has emerged as the most effective, efficient, and promising choice in green sustainability practices. ZnO is a wurtzite-structured white hexagonal crystal. Photocatalysis, cosmetics, paint industries, ceramics, organic synthesis, and fertilisers are just a few of the uses for this promising semiconductor material. By regulating the band gap and expanding the surface area, it has been discovered that modifying ZnO with various metal and non-metal dopants improves photocatalytic efficiency [38–40].

Numerous metals, such as Cu, Fe, Al, Nd, Gd, Ag, Sn, Mn, In, Mg, Au, Ti, and others, are recurrently used as doping agents in ZnO, but nickel is found to be effective dopant as it promotes visible light absorption by bringing down the band gap, emits electron-hole pairs, declines the recombination of these photo-induced charge carriers, provides strength and stability, improves morphological characteristics, and endorses the principal metal oxide for the photocatalytic degradation [38,41]. A base metal oxide's energy levels are unaffected by a dopant concentration that is too low and on the other hand its original nature is altered by a dopant concentration that is too high. Consequently, using the ideal dopant concentration is crucial for efficient doping. The photocatalytic capabilities of the metal oxide photocatalysts are discovered to be enhanced by the 5 % metal dopant concentration [38].

The therapeutic potential of nanoparticles in the realm of bio-nano medicine to treat diseases is promising [42–46]. To combat the issue of antimicrobial resistance, several antimicrobial agents have been designed and are being targeted [47–49]. In addition to successfully developing novel antimicrobial drugs, organic chemists are aiming to synthesize a range of powerful heterocyclic compounds [50–54]. The research from the previous decade has demonstrated that ZnO antimicrobials can also be used as effective antibacterial agents.

Gram-positive, spherically shaped *Staphylococcus aureus* (*S. aureus*), a member of the Bacillota, is frequently found in the upper respiratory tract and on the skin [55–57]. *S. aureus* is a very common human pathogenic microorganism that can cause a variety of infectious diseases, including skin and soft tissue infections, and lethal pneumonia also [57]. *S. aureus* could be classified as methicillin-sensitive *Staphylococcus aureus* (MSSA) and methicillin-resistant *Staphylococcus aureus* (MRSA) [57]. Smaller sized nanoparticles have higher biological activity due to their increased surface area bound to cell surface, which is a crucial factor in biomedical activities that depend on NP size. Furthermore, an appropriate concentration of dopant on biomedical implants must be used in order to have good antibacterial action without having a cytotoxic influence [58]. By considering all above vital aspects, herein we wish to report efficient photocatalytic degradation of eosin blue dye and antibacterial study using nanostructured zinc oxide and 5 % nickel modified zinc oxide. The synthesized ZnO and Ni/ZnO nanomaterials are successfully characterized by XRD, SEM, EDS, UV–Vis, and FT-IR techniques and employed for EB dye photocatalysis and antibacterial screening against *S. aureus*. The Ni/ZnO nanomaterial is found to be efficient material for photocatalysis and antibacterial activity as compared to bare ZnO.

2. Materials and methods

Analytical grade (AR) reagents (Make: SD Fine chemicals) were purchased from a local source for this study. The chemicals had a purity of 99.99 percent and thus used without further purification. The authors used Zn $(NO_3)_2.6H_2O$, Ni$(NO_3)_2.9H_2O$, sodium hydroxide (NaOH), and deionized water. The general characteristics of the EB dye utilised in this work are depicted in Fig. 1.

2.1. Synthesis of undoped ZnO nanomaterial by co-precipitation method

The undoped ZnO nanomaterial was made using a standard co-precipitation method. Zinc nitrate and sodium hydroxide were utilised as precursors. A 0.01 M aqueous zinc nitrate solution is created in 100 mL deionized water during the synthesis of zinc oxide. Drop by drop, at 80 °C, 0.01 M NaOH solution was added to the zinc precursor solution until the full 50 mL of NaOH was used to raise the pH of the reaction up to 12. After complete addition of sodium hydroxide, the white coloured precipitate of zinc hydroxide was generated, this was whirled at 2500 rpm for 30 min. The resultant solution was filtered using Whatman filter paper number 41. The resulting residue was rinsed two to three times with hot water to remove any contaminants. The precipitate was dried under an infrared light, then transferred to a silica crucible and calcined in a muffle furnace at 550 °C for 4 h. The white zinc oxide nanoparticles from the muffle furnace were recovered the next day. The produced ZnO nanoparticles were characterised and further investigation was conducted.

2.2. Synthesis of Ni/ZnO nanomaterial by co-precipitation method

Ni/ZnO nanomaterial was also synthesised using the same co-precipitation process. The main technique for synthesising Ni/ZnO was the same as described in section 2.1, with the exception of adding nickel nitrate as a dopant during the synthesis of zinc oxide nanoparticles. Nickel nitrate was added at a rate of 5 mol percent during the manufacture of Ni/ZnO. The faint green Ni/ZnO nanoparticles were synthesised using the entire procedure described in section 2.1, with the addition of 5 % nickel nitrate.

2.3. Antibacterial activity

Agar well difusion assay was used for antibacterial activity of ZnO and Ni/ZnO nanomaterials against *S. aureus* as per previously reported method [58]. The antibacterial activity was taken in 25, 50 and 100 μg/mL concentrations. In a typical procedure, each dried paper disk (Whatman filter paper No.1) contained synthesized ZnO and Ni/ZnO nanomaterials in 25, 50 and 100 μg/mL concentrations. Each disk was then placed on the surface of the sterile solidified respective agar medium which was spread with 24 h old inoculums. The plates were kept in the refrigerator for diffusion for 3 h and then transferred to the incubator at 37 ℃ for 24–48 h. After incubation, the zones of inhibition around the discs were measured by the zone scale. .

3. Results and discussions

3.1. Characterization of ZnO and Ni modified ZnO

3.1.1. UV–Vis absorption studies

The UV–Vis absorption spectra of ZnO and Ni/ZnO nanomaterials were recorded using UV–Visible-NIR-DRS Spectrophotometer V770, JASCO, Japan. The UV–Vis spectroscopic technique is powerful tool to access the band gap energy and to affirm the formation of nanomaterials. The specific nanomaterials show specific absorption and thus its formation can be efficiently predicted. Moreover, the occurrence of a

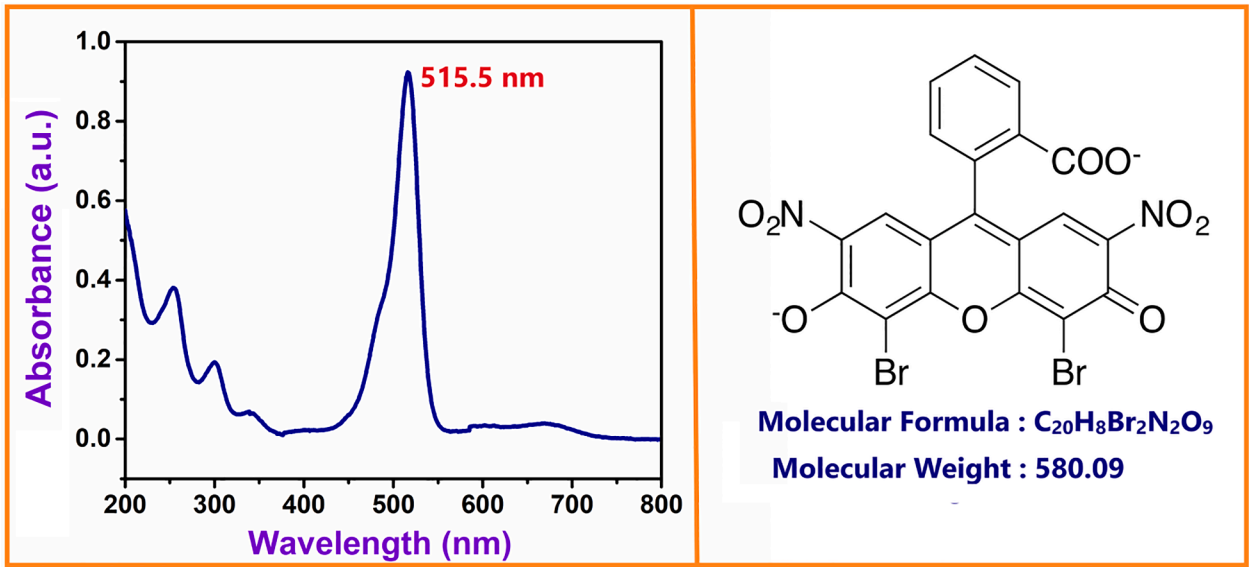

Fig. 1. General characteristics of EB dye used in present research.

red shift could be a sign that surface modification is accomplished. Fig. 2a-b shows the absorption spectra of synthesized ZnO and Ni/ZnO nanomaterials. On the other hand, the Tauc plots are depicted in Fig. 2c-d for synthesized ZnO and Ni/ZnO nanomaterials. By observing the UV–Vis spectra and Tauc plots, it has been clearly assigned that nickel dopant has shifted the absorption maxima to a longer wavelength

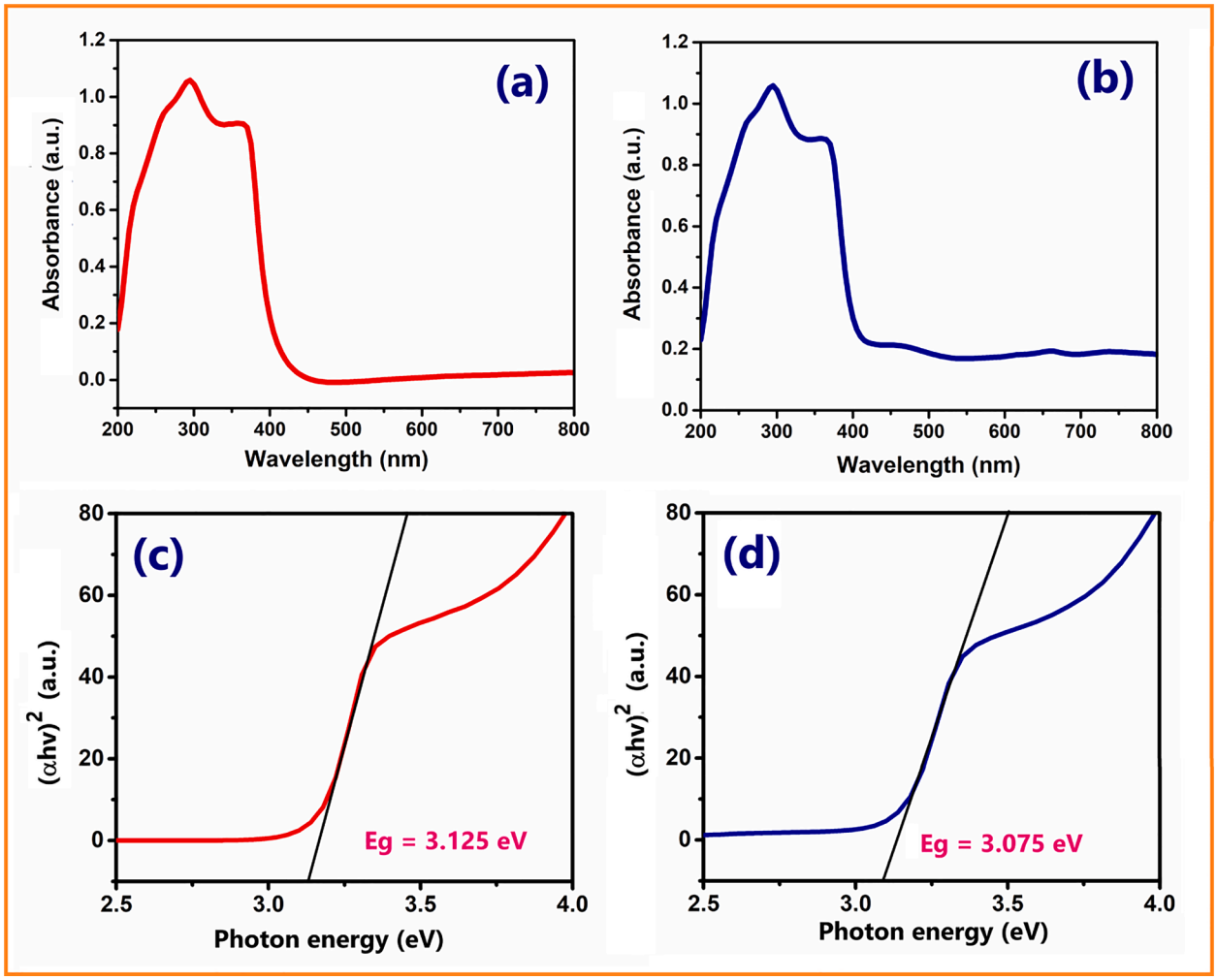

Fig. 2. a-b UV/Visi absorption spectra of ZnO and Ni/ZnO nanomaterials and c-d Tauc plots of ZnO and Ni/ZnO nanomaterials.

thereby showing bathochromic shift (red shift). ZnO and Ni/ZnO are having band gap 3.125 eV and 3.075 eV. The band gap is vital parameter for photo excitation of electrons. Lower the band gap greater will be the photo excitation of electrons. The nanomaterials with lower band gap are found to show higher photocatalytic activity than those with higher band gap. The improved visible light absorption of EB dye in the present work is owing to the generation of more photo-excited electrons in the Ni/ZnO nanomaterial, which may boost EB dye degradation efficiency. The UV–Vis spectrum data clearly revealed that a significant red shift had occurred in the Ni/ZnO nanomaterial when compared to the undoped ZnO nanomaterial. The red shift is assumed to be caused by the presence of nickel doping. The narrowed band gap suggests that electron transport is inevitable, allowing for facile photocatalysis of the EB dye.

3.1.2. FT-IR analysis

FT-IR spectroscopic analysis is one of the powerful tool to determine the presence of various kinds of functional groups and chemical bonding in wide sorts of compounds. FT-IR spectra of ZnO and Ni/ZnO nanomaterials were recorded by FTIR Spectrometer 4600, JASCO, Japan. The measurements were taken in the range of 400–4000 cm^{-1}. The obtained FT-IR spectra of FT-IR spectra of ZnO and Ni/ZnO nanomaterials are given in Fig. 3. The presence of ZnO band is found at 439.69 cm^{-1} in ZnO and at 426.191 cm^{-1} in Ni/ZnO. The lowering in absorption band is attributed to Ni doping into ZnO nanomaterial. No water absorption peaks in both FT-IR spectra confirms the absence of water molecules over the surface of prepared nanomaterials.

3.1.3. X-ray diffraction study

Fig. 4a and b show the XRD patterns for undoped ZnO and Ni/ZnO. CuK1 radiations with a wavelength of 1.54°are utilised to generate the X-rays, and the Braggs scanning angle on the XRD equipment ranges from 10 to 90°. According to the data obtained from XRD investigation, the produced materials belong to the traditional hexagonal wurtzite ZnO lattice. The Braggs' reflection peaks are linked to the development of hexagonal wurtzite ZnO lattice. According to the XRD investigation, the diffraction peaks for the ZnO material are 31.91°, 34.49°, 36.25°, 47.61°, 56.69°, 62.97°, 68.03°, 69.20°, and 72.65°. The reflection of typical hkl planes such as (100), (002), (100), (102), (110), (103), (200), (112), and (201) planes would be attributed to the 2θ values. The average grain size was calculated using Scherer's formula. Using the Debye-formula, Scherer's, the average grain size for undoped ZnO was calculated to be 23.25 nm, while the average grain size for Ni/ZnO was calculated to be 20.75 nm.

3.1.4. Scanning electron microscopy study

The morphological properties of ZnO and Ni/ZnO materials were examined using scanning electron microscopy (SEM). SEM is beneficial

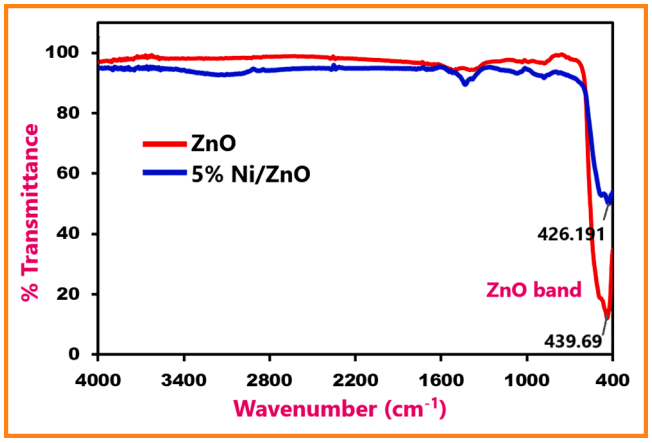

Fig. 3. FT-IR spectra of ZnO and Ni/ZnO nanomaterials.

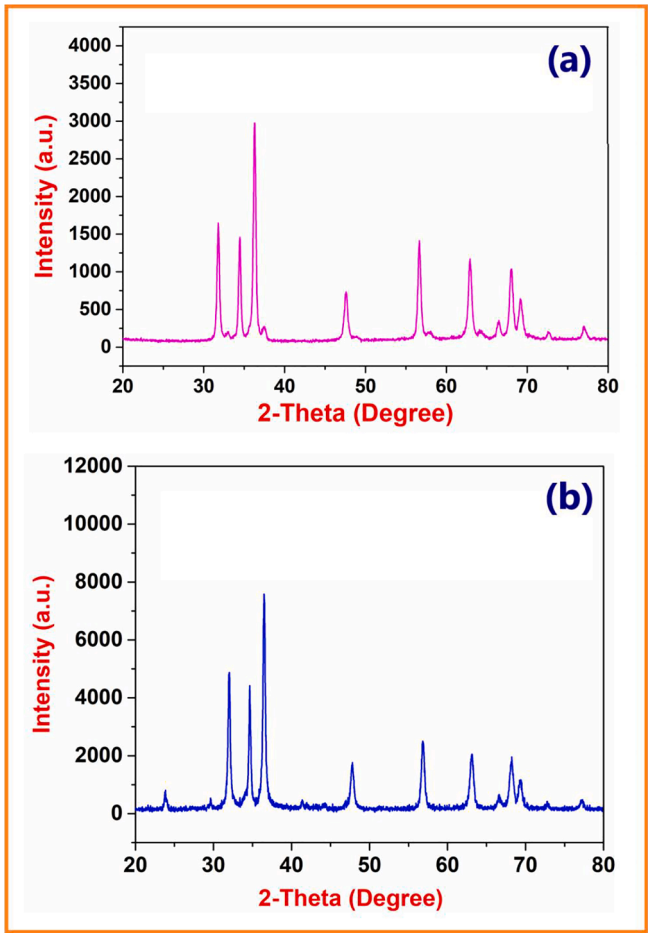

Fig. 4. XRD pattern for undoped ZnO (a) and Ni/ZnO (b).

for examining the morphological characteristics of the processed material, such as texture, porosity, and crystal grain appearance. SEM micrographs of ZnO are shown in Fig. 5a-b, while SEM micrographs of Ni/ZnO are shown in Fig. 5c-d. As seen in SEM pictures, the resulting material has diverse size pores along the lattice; grains of various sizes are thickly agglomerated together. Based on SEM scans, the material looks to be porous. The produced materials are suitable for photocatalytic research because they contain pore or interstitial gaps of various sizes throughout the surface lattice. The materials' porosity is an important characteristic for trapping dye molecules. For an effective redox mechanism, the dye fragments are retained in place by the interstitial gaps, and dye degradation happens quickly. As a consequence, the produced catalyst is effective in photocatalytically removing EB dye.

3.1.5. Energy dispersive spectroscopy study

Energy dispersive spectroscopy (EDS) was used to analyse the chemical composition of the produced catalysts. Fig. 6a-b shows the EDS spectra for undoped ZnO and Ni/ZnO, respectively. The doping % was validated by EDS because the zinc oxide material was doped with iron. The EDS spectrum for 5 percent Ni modified ZnO is shown in Fig. 6b. From the spectrum, the peaks for iron and zinc are plainly visible. At 9.0 KeV, elemental zinc resoluted, while elemental iron resoluted at 6.4 KeV. In the inset image of Fig. 6b, the chemical composition of iron modified ZnO is shown. As expected, the elemental composition is found as expected.

3.2. Photocatalysis study

The photocatalysis utilizing undoped ZnO and Ni/ZnO over EB color

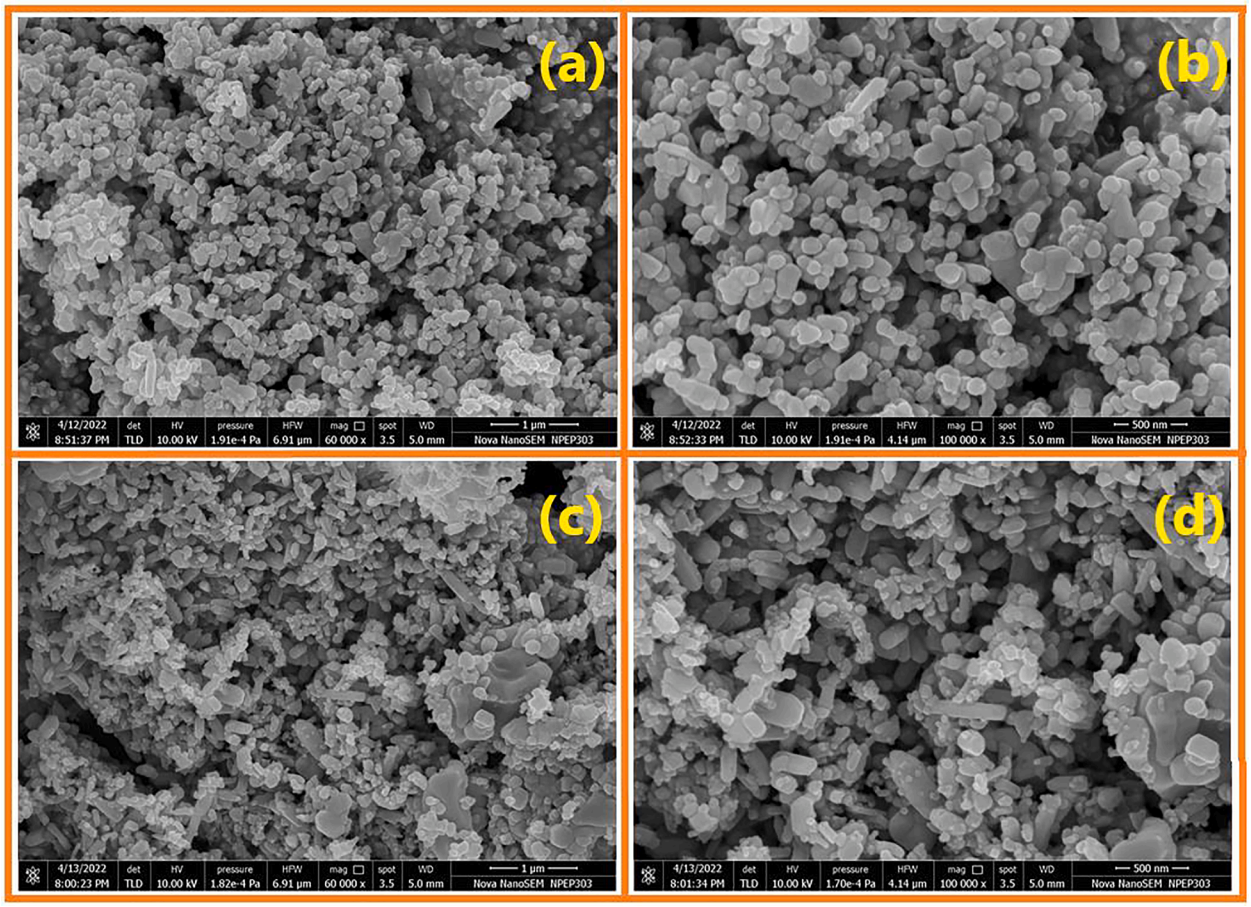

Fig. 5. (a-b) SEM micrographs of undoped ZnO; (c-d) Ni/ZnO material.

was inspected. A photocatalytic reactor with mercury light with a force of 260 Watts was utilized to research the photocatalytic debasement of EB color. UV spectrophotometer with an UV scope of 200–800 nm was utilized to quantify changes in EB color fixation. Another significant variable that decides if colors debase in acidic or fundamental conditions is pH. After centrifugation, the last absorbance of the supernatant color fluid was estimated to stay away from obstruction from impetus particles. Eosin blue color photocatalytic debasement was assessed to happen at a wavelength of max 520 nm. The fundamental boundaries were fixed after an intensive examination of the multitude of variables for EB color debasement at undoped Ni/ZnO. The dye concentration was set at 20 ppm, pH = 8.0, and nanocatalysts fixation was 0.8 g/L. The accompanying optimization addresses the general parameters of photocatalytic debasement of EB color.

3.2.1. *Effect of catalyst dose on % degradation of EB dye*

One of the most important parameters in the photocatalysis investigation is the catalyst dose optimization. The effect of catalyst dose on percent degradation of EB dye using ZnO and Ni/ZnO is shown in Fig. 7a and 7b, respectively. The catalyst dose was changed from 0.2 to 1.0 g/L for both bare ZnO and Ni/ZnO to better understand the optimal catalyst dose. For this trial, the dye concentration was increased from 20 to 60 ppm. It was discovered that when the catalyst dose was increased, both ZnO and Ni/ZnO displayed good photocatalytic activity. The catalyst dosages of 0.8 g/L and 1.0 g/L were shown to be superior in terms of photocatalytic efficiency. For ZnO and Ni/ZnO, photocatalytic degradation was accomplished at 95 percent and 97 percent for 0.8 g/L catalyst dosage, respectively. However, the increase in photocatalytic degradation was just 1 % at 1.0 g/L catalyst dosage. It was obvious that a catalyst dose of 0.8 g/L was optimal for photocatalytic degradation of EB dye. The photodegradation effectiveness of both bare ZnO and Ni/ZnO was observed to decrease as the concentration was increased from 20 ppm to 60 ppm.

3.2.2. *Effect of change in pH on % degradation of EB dye*

The catalyst surface is greatly affected by change in pH. So it was important see the effect of change in pH on % degradation of EB dye. Before investigating the effect of pH, we determined zero point charge (ZPC) of the Ni/ZnO. TO determine the ZPC, the pH range was set from 5 to 12 in eight reaction vessels using 0.1 M HCl and 0.1 M NaOH solutions, with 0.1 g of fixed catalyst added to each reaction vessel. The reaction vessels were then kept as it is for 24 h after adding the catalyst, and the pH of each reaction vessel was then measured. The graph demonstrates the variation between the fixed pH and the pH after 24 h. For each catalyst, the intercepting point is the ZPC. The ZPC value for Ni/ZnO was predicted to be 7.4.The graphs of variation in pH for both photocatalysts are as represented in Fig. 8. At pH < pH_{ZPC} the catalyst surface is positively and hence it attracts the negative dye species. Hence the dyes carries net negative charge would attracted between this ranges their degradation is expected within pH_{ZPC} value. But, in this investigation EB dye being basic in nature has net positive charge and expected to be attracted in the pH > pH_{ZPC}, i.e in the basic range from 7.4 onwards. As per the results obtained the % degradation of EB dye is very slow from 5 to 7 pH as represented in Fig. 8. But with increment in pH beyond 7the rapid degradation from 7 to 8.0 pH was observed. The lower degradation of EB dye below ZPC is attributed to the positive surface. The repulsion between positive surface of ZnO, Ni doped ZnO and positively charge EB dye creates electrostatic repulsive force. Hence EB dye molecules do not form the constructive bonding between positively charge catalyst surface and EB dye. Ultimately this repulsive force

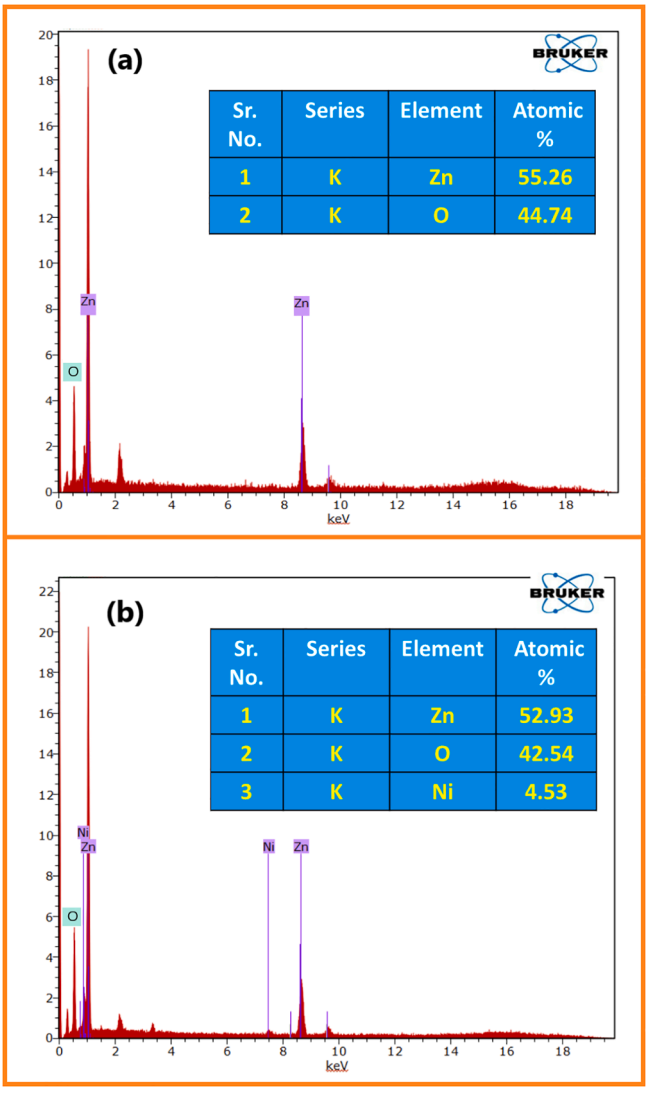

Fig. 6. (a) EDS spectrum of undoped ZnO material, (b) Ni/ZnO material.

is responsible to lower degradation at pH < pH_{ZPC}.

3.2.3. *Effect of initial dye concentration*

The dye concentration assessment is a crucial part of the photocatalysis investigation in order to set the ideal degradation parameter. This metric is useful for determining the reaction's overall contact time and rate. The EB dye concentration was varied from 10 mg L^{-1} to 90 mg L^{-1} (10 ppm to 90 ppm) in this study, with the optimum catalyst dose of 0.8 g keeping constant for all EB dye concentrations. The rate of degradation by the evaluated catalyst for EB decreased as the concentration of EB dye increased from 10 ppm to 90 ppm, according to the overall dye concentration analysis. As the concentration of EB dye increases, so does the accumulation of EB dye on the catalyst's surface, which causes quenching between the upper energy state of EB molecules. As a result, photocatalytic degradation of EB dye reduces as concentration rises. Furthermore, due to the buildup of dye particles on the catalyst surface, an increase in EB dye concentration prevents photons from irradiation light from coming into direct contact with the catalyst surface. The addition of more dye particles on catalyst surfaces reduces the active sites of catalysts. With an increase in EB dye concentration, the photocatalytic degradation is shown to be reduced due to catalyst inactivity. Fig. 9 shows a diagrammatic representation of the influence of initial dye concentration.

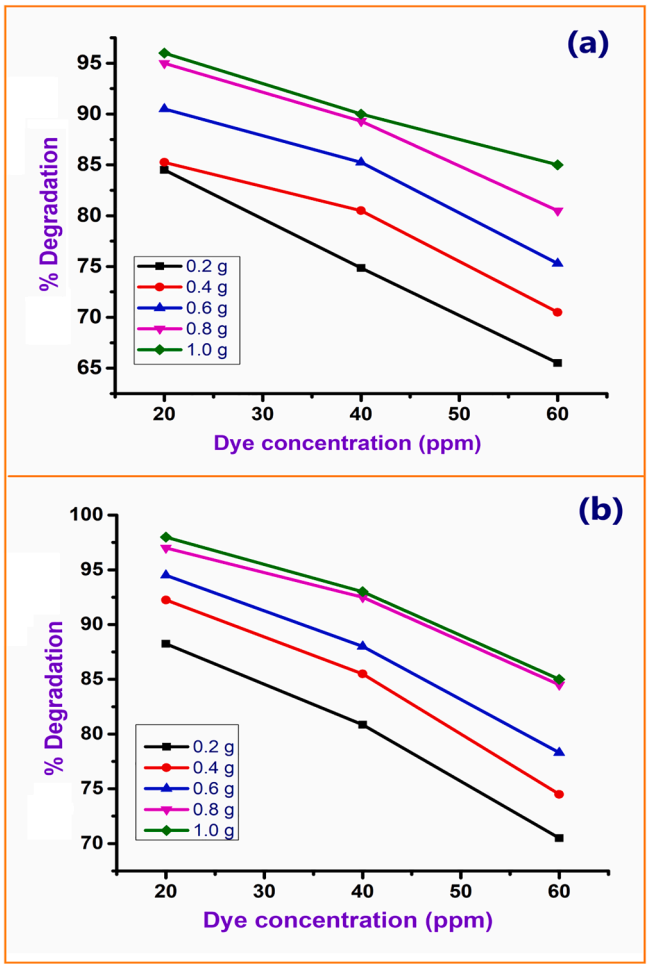

Fig. 7. (a) Effect of ZnO catalyst dose on % degradation of EB dye for 20, 40 and 60 ppm EB dye concentrations, (b) Effect of Ni/ZnO catalyst dose on % degradation of EB dye for 20, 40 and 60 ppm EB dye concentrations.

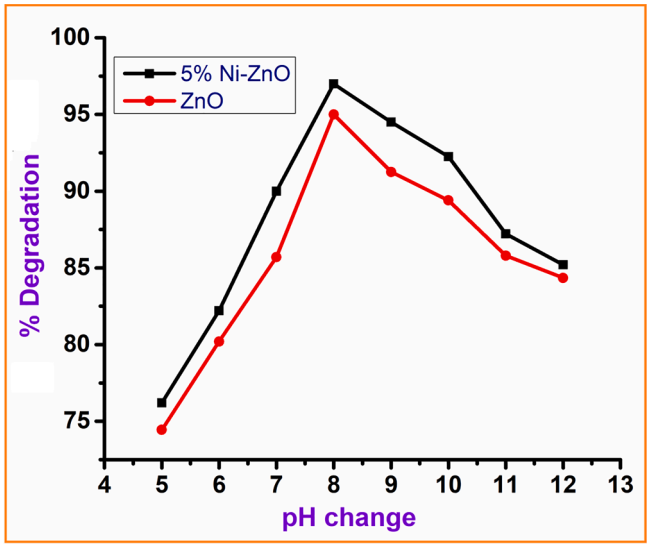

Fig. 8. Effect of pH on degradation of EB dye for undoped ZnO and Ni/ZnO.

3.2.4. *Contact time study*

The contact time investigation is a key parameter that determines the real time necessary for photocatalytic dye degradation at various dye

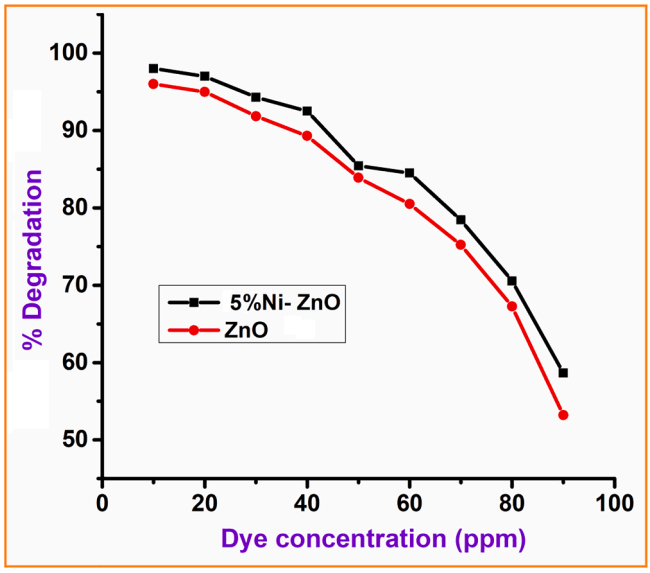

Fig. 9. Effect of initial dye concentration for degradation EB dye for undoped ZnO and Ni/ZnO at 0.8 g/L and pH 8.0.

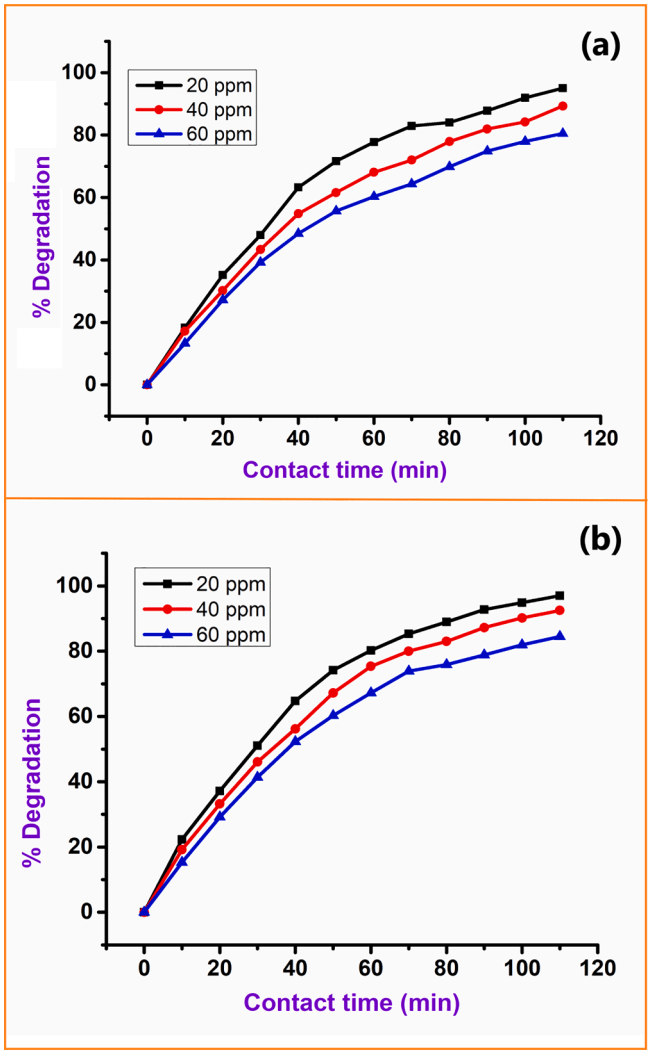

Fig. 10. (a) Contact time study for EB dye degradation at undoped ZnO, (b) Contact time study for EB dye degradation at Ni/ZnO at pH = 8.0, catalyst dose 0.8 g/L.

concentrations. Fig. 10 a-b shows the effect of contact time for various concentrations of EB dye ranging from 20 mgL^{-1} to 60 mgL^{-1}. The dye degrades quickly at first, with about 80 % of the EB dye destroyed in 110 min. The breakdown of EB dye occurs at a higher pace in the early stages due to the presence of more surface active sites on the undoped and doped ZnO catalysts. These surface active sites encourage the catalyst to degrade at a faster rate. As photocatalysis progresses, dye particles or molecules accumulate on the catalyst surface, limiting the effective photon impacting the catalyst surface. With a larger concentration of EB dye, the accessible active sites and effective photon interaction diminish even more, and therefore the photocatalytic degradation of EB dye declines with increasing EB dye concentration and time. The catalyst dose of 0.8 g/L, pH = 8.0, and EB dye concentration of 20 mg/L are the conditions established for successful degradation of the overall concentration of EB dye. The entire contact time for the reaction is 110 min when all of these parameters are kept constant. Overall mineralization of the EB dye can be seen at this point.

3.2.5. *Detection of ROS by scavenging study*

Reactive oxygen species (ROS) are formed during photocatalysis and play an important part in the dye degradation process. Hydroxide radicals (OH^-), $\bullet O^{2-}$, h^+, and other ROS are the most common. Scavengers are mostly used to catch ROS in order to affirm the formation of ROS production. Benzoquinone (BQ = $\bullet O_2$ scavenger) and isopropyl alcohol (IPA = •OH scavenger) are the most often employed species for capturing these ROS species. The Ni/ZnO catalyst was subjected to a scavenging examination in this work. Fig. 11 depicts the total scavenging study outcome. When the scavenger IPA was added to the reaction vessel holding the Ni/ZnO catalyst with a specified EB dye concentration, the rate of photocatalytic degradation was initially found to be declining. In the presence of a benzoquinone scavenger, the rate of EB dye degradation was shown to be higher than that of IPA. According to the results of the overall experiment, the formation of ROS is trapped by scavengers; resulting in a decrease in the photocatalytic degradation of EB dye for a Ni/ZnO catalyst.

3.2.6. *Reusability performance of prepared photocatalyst*

The reusability test is a key characteristic for confirming the repeatability of the produced catalyst's test findings. The synthesised catalyst in this work, a Ni/ZnO catalyst, was used for reusability testing under UV–Visible illumination with a 260 W voltage and the optimal parameters of tested EB concentration of 20 ppm, pH = 8.0, and catalyst dose of 0.8 g/L. The catalyst was initially recovered from the reaction

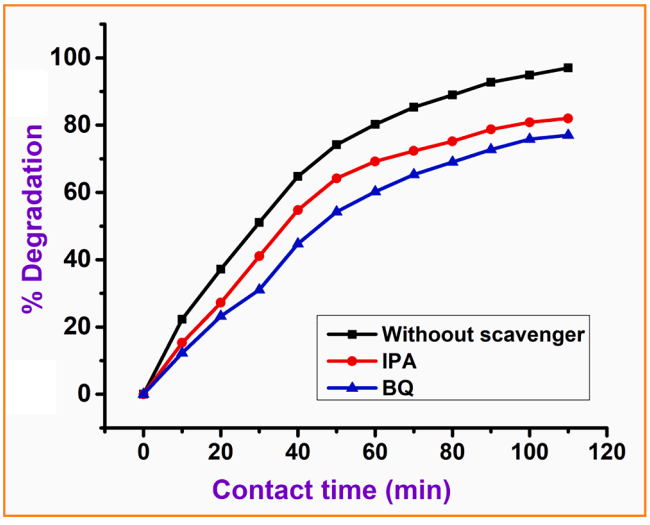

Fig. 11. Radical scavenging studies for EB dye at 5% Ni doped ZnO photocatalyst.

vessel that had been left following the contact time research. The solution containing Ni/ZnO catalyst was centrifuged and then Ni/ZnO filtered with Whatman filter paper 41, then washed with ethyl alcohol and hot water, and dried for 30 min under an IR lamp and calcined at appropriate temperature. For the reusability test, the dried catalyst was used. To reach a firm conclusion of the acquired results, the reusability test was run four times. The EB dye degradation was observed to be 97 percent in the first run using a Ni/ZnO catalyst. Before commencing the second run, the catalyst was removed from the reaction vessel and dried using the same technique as previously described. After refining the reaction conditions, the EB dye degradation was determined to be 95.3 % in the second run. The percent degradation of EB dye for the same recovered catalyst was determined to be 93.1 % and 90.7 % in the third and fourth runs, respectively. The total degradation analysis revealed that the Ni/ZnO nanoparticles are very stable and robust catalysts when it comes to the breakdown of EB dye, with insignificant percent degradation variation. The drop in EB dye in each run can be attributed to a decrease in catalyst surface activity due to much usage, a decrease in surface area, and a drop in catalyst concentration during the filtration process. Based on the results of the overall reusability test, Ni/ZnO catalysts are highly effective, accessible, and stable catalysts for EB dye degradation. Fig. 12 shows the reusability findings while using EB dye.

3.2.7. Photocatalytic reaction mechanism

Fig. 13 depicts a possible photocatalytic reaction pathway for dye degradation utilising Ni/ZnO as per previously reported literature [41]. The active species in the photocatalytic degradation of EB dye solution include hydroxyl radicals, photogenerated holes, and superoxide radical anions. The photocatalytic breakdown of organic dyes is dominated by hydroxyl radicals and photogenerated holes. Under UV light, electrons in ZnO's valence band (VB) are driven to go to the conduction band (CB), while the VB releases the same amount of holes (h+). Nickel being an *n*-type of semiconductor and base metal oxide ZnO is p-type of semiconductor. Nickel forms continuum near conduction band of ZnO resulting in decrease in optical band gap and form strong p-n junction for the ejection of electrons from the valence band. Moreover, the Fermi levels of nickel have different energies than ZnO levels so electrons trap for longer time in these levels and available for the generation of ROS's in aqueous medium. Literature confirms that as an optical band gap decreases and it raises HOMO levels and decreases LUMO levels in semiconducting material after doping which is an ideal scenario for the generation of photo induced charge carries (e-/h+). Dissolved oxygen in aqueous solution functions as an electron scavenger, reacting with electrons to form active free radicals such as OH, O^{2-}, and others. The electron donors (H_2O) will react with the separated holes to form active OH free radicals. Following that, the generated h+ and other free radicals such as OH, O^{2-}, and others attacked surface-adsorbed EB molecules, resulting in discoloration and opening-ring reactions.

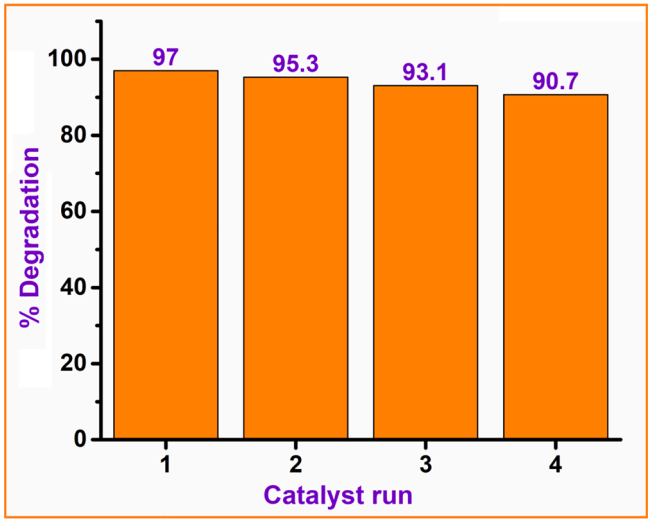

Fig. 12. Reusability study of Ni/ZnO for EB dye degradation.

3.2.8. Comparison of the prepared catalyst

ZnO-based materials and nanocomposites are employed for photocatalytic degradation of various dyes, azo dyes, insecticides, herbicides, colour shades, effluent from pharmaceutical and chemical waste, and industrial effluents. The photocatalysis comparison is based on similar types of ZnO-based materials that have been employed as photocatalysis for the degradation of various pollutants and dyes reported by researchers so far. The produced catalyst was used as a photocatalyst to degrade the EB dye. The results for the degradation of EB dye at 20 ppm dye concentration in a somewhat alkaline environment with a contact period of 110 min and a catalyst dose of 0.8 g/L are highly promising. Table 1 shows the results of a comparative investigation of photocatalytic degradation of several colours against ZnO-based materials.

3.3. Antibacterial activity

The antibacterial activity of synthesized ZnO and Ni/ZnO nanomaterials was investigated by the Agar diffusion method. The antibacterial action of ZnO and Ni/ZnO nanomaterials were tested against *S aureus* and the results are depicted in Fig. 14. The synthesized nanomaterials are found to inhibit the growth of *S aureus.* The antibacterial activity was taken in 25, 50 and 100 μg/ML concentrations. The antibacterial activity was found to increase from lower concentration to higher concentration. Importantly, it has been found the Ni/ZnO nanomaterial possessing comparatively more potent antibacterial action than bare ZnO. Consequently, Ni/ZnO can be used as an effective antibacterial agent with further modifications.

Conclusions

Eosin blue dye degradation was revealed to be very promising by employing Ni/ZnO nanomaterial. According to current findings, the Ni/ZnO nanomaterial degrade the EB dye with high efficacy and a short time span, which is a positive step towards environmental treatment applications in laboratory scale batch procedures. Effect of catalyst dose, effect of pH, effect of dye concentration and scavenging study are key highlights of the present study. The 0.8 g/L catalyst dose was found to be optimum for 97 % degradation of EB dye within 110 min at pH = 8.0. The scavenging study using IPA and BQ revealed the presence of ROS as active species in the photocatalysis. Numerous virtues, such as plenty of voids over catalyst surface, concise photoelectric conductivity, sufficient active sites, and high surface area, are attributed to the excellent photocatalytic activity of Ni/ZnO towards the EB dye, implying that the material has excellent potential in actual contaminated water treatment. Importantly, the synthesized Ni/ZnO is found to be good antibacterial agents against *S. aureus*. As a result, present investigation suggested that nickel modification over ZnO has been proven to be successful, and it can be employed in environmental as well as antibacterial applications.

Funding Information

The authors declared that they not received any grant from any funding agency for the present research work, the present work is self-funded.

CRediT authorship contribution statement

Mansi H. Magar: Methodology, Validation, Formal analysis, Investigation, Data curation, Writing – original draft, Writing – review & editing, Visualization. **Vishnu A. Adole:** Conceptualization, Methodology, Software, Validation, Formal analysis, Investigation, Data curation,

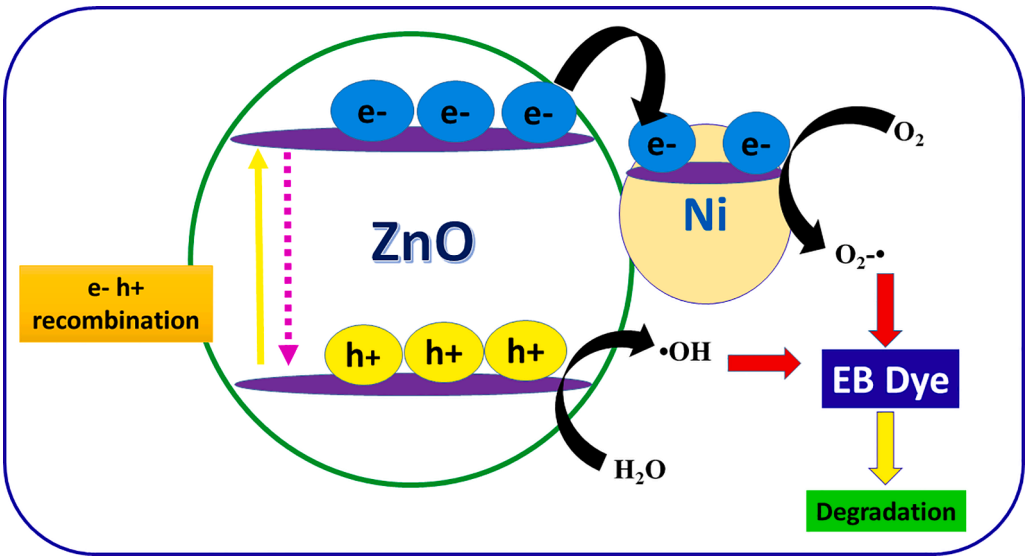

Fig. 13. Photocatalytic reaction mechanism.

Table 1
Comparative study of Ni/ZnO catalyst against the ZnO based materials for the reported photocatalytic degradation of eosin blue dye.

Entry	Nanomaterial used	Dye Conc. (ppm)	Catalyst dose (g/L)	Time (Min)	% Degradation	Reference
1.	1.5 %Nd-Gd/ZnO	20	0.1	120	93	[59]
2.	Al-Fe/ZnO	10	1	75	90	[60]
3.	NiO–ZnO–Ag	10	0.02	90	94	[61]
4.	3 % Gd/ZnO	10	0.33	90	93	[62]
6.	5% Ni/ZnO	20	0.8	110	97	Present work

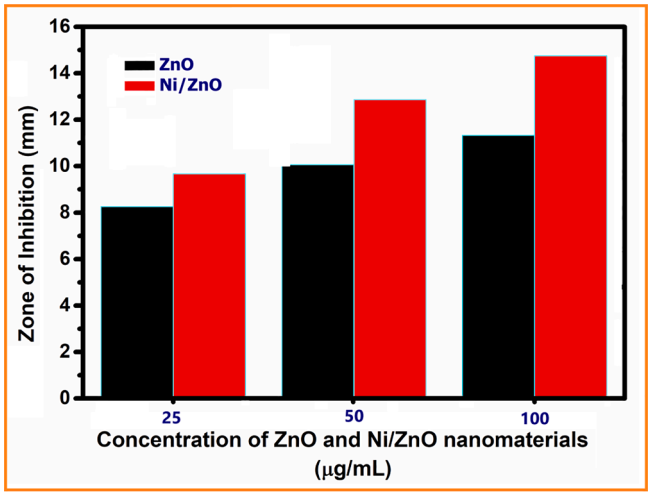

Fig. 14. Antibacterial activity of synthesized nanomaterials against *Staphylococcus aureus*.

Writing – original draft, Writing – review & editing, Visualization, Supervision. **Ravindra H. Waghchaure:** Conceptualization, Methodology, Software, Validation, Formal analysis, Investigation, Data curation, Writing – original draft, Writing – review & editing, Visualization, Supervision. **Thansing B. Pawar:** Conceptualization, Methodology, Software, Validation, Formal analysis, Investigation, Data curation, Writing – original draft, Writing – review & editing, Visualization, Supervision.

Declaration of Competing Interest

The authors declare that they have no known competing financial interests or personal relationships that could have appeared to influence the work reported in this paper.

Data availability

No data was used for the research described in the article.

Acknowledgments

Authors are gratefully acknowledged to CIF, SPPU, Pune for SEM and EDS study, STIC Kochin for XRD and Jaysingpur College, Kolhapur for UV and FT-IR characterization facility. Authors are also very much thankful to Research Centre in Chemistry, LVH Arts, commerce and Science College, Panchavati, Nashik for laboratory facilities.

References

[1] W.J. Stark, P.R. Stoessel, W. Wohlleben, A.J.C.S.R. Hafner, Industrial applications of nanoparticles, Chem. Soc. Rev. 44 (16) (2015) 5793–5805.
[2] I. Khan, K. Saeed, I. Khan, Nanoparticles: Properties, applications and toxicities, Arabian J. Chem. 12 (7) (2019) 908–931.
[3] S. C Thomas, P. Kumar Mishra, S. Talegaonkar, 2015. Ceramic nanoparticles: fabrication methods and applications in drug delivery. Curr. Pharmaceutical Design, 21(42), pp.6165-6188.
[4] M.S. Tufail, I. Liaqat, 2021. 2. Silver nanoparticles and their applications-a comprehensive review. Pure and Applied Biology (PAB), 11(1), 315-330.
[5] M.N. Atalar, A. Baran, M.F. Baran, C. Keskin, N. Aktepe, Ö. Yavuz, S. İrtegun Kandemir, Economic fast synthesis of olive leaf extract and silver nanoparticles and biomedical applications, Part. Sci. Technol. (2021) 1–9.
[6] S.B. Singh, Emerging sustainable nanomaterials and their applications in catalysis and corrosion control, Curr. Nanosci. 17 (4) (2021) 540–553.
[7] S.D. Anderson, V.V. Gwenin, C.D. Gwenin, Magnetic functionalized nanoparticles for biomedical, drug delivery and imaging applications, Nanoscale Res. Lett. 14 (1) (2019) 1–16.
[8] L. Gloag, M. Mehdipour, D. Chen, R.D. Tilley, J.J. Gooding, Advances in the application of magnetic nanoparticles for sensing, Adv. Mater. 31 (48) (2019) 1904385.

[9] V.A. Adole, T.B. Pawar, P.B. Koli, B.S. Jagdale, Exploration of catalytic performance of nano-La2O3 as an efficient catalyst for dihydropyrimidinone/thione synthesis and gas sensing, J. Nanostructure Chem. 9 (1) (2019) 61–76.

[10] R.S. Shinde, S.D. Khairnar, M.R. Patil, V.A. Adole, P.B. Koli, V.V. Deshmane, D. K. Halwar, R.A. Shinde, T.B. Pawar, B.S. Jagdale, A.V. Patil, Synthesis and characterization of ZnO/CuO nanocomposites as an effective photocatalyst and gas sensor for environmental remediation, J. Inorg. Organomet. Polym Mater. (2022) 1–22.

[11] D. Cheng, H.H. Ngo, W. Guo, S.W. Chang, D.D. Nguyen, Y. Liu, Q. Wei, D. Wei, A critical review on antibiotics and hormones in swine wastewater: Water pollution problems and control approaches, J. Hazard. Mater. 387 (2020), 121682.

[12] A. Fröse, K. Schmidtke, T. Sukmann, I.J. Junger, A. Ehrmann, Application of natural dyes on diverse textile materials, Optik 181 (2019) 215–219.

[13] M. Gastaldi, F. Cardano, M. Zanetti, G. Viscardi, C. Barolo, S. Bordiga, S. Magdassi, A. Fin, I. Roppolo, Functional dyes in polymeric 3D printing: applications and perspectives, ACS Mater. Lett. 3 (1) (2020) 1–17.

[14] S. Kalpana, S.R. Priyadarshini, M.M. Leena, J.A. Moses, C. Anandharamakrishnan, Intelligent packaging: Trends and applications in food systems, Trends Food Sci. Technol. 93 (2019) 145–157.

[15] P.B. Koli, K.H. Kapadnis, U.G. Deshpande, Study of physico-chemical properties, detection and toxicity study of organic compounds from effluent of MIDC Thane and GIDC Ankleshwar industrial zone, Appl. Water Sci. 8 (7) (2018) 1–9.

[16] S. Sahu, S. Pahi, S. Tripathy, S.K. Singh, A. Behera, U.K. Sahu, R.K. Patel, Adsorption of eosin blue on chemically modified lychee seed biochar: Dynamic, equilibrium, and thermodynamic study, J. Mol. Liq. 315 (2020), 113743.

[17] N. Tara, S.I. Siddiqui, G. Rathi, S.A. Chaudhry, A.M. Asiri, Nano-engineered adsorbent for the removal of dyes from water: A review, Curr. Anal. Chem. 16 (1) (2020) 14–40.

[18] A. Muniyasamy, G. Sivaporul, A. Gopinath, R. Lakshmanan, A. Altaee, A. Achary, P.V. Chellam, Process development for the degradation of textile azo dyes (mono-, di-, poly-) by advanced oxidation process-ozonation: experimental & partial derivative modelling approach, J. Environ. Manage. 265 (2020), 110397.

[19] M.R. Patil, V.S. Shrivastava, Adsorption of malachite green by polyaniline–nickel ferrite magnetic nanocomposite: an isotherm and kinetic study, Appl. Nanosci. 5 (7) (2015) 809–816.

[20] M.B. Ceretta, Y. Vieira, E.A. Wolski, E.L. Foletto, S. Silvestri, Biological degradation coupled to photocatalysis by ZnO/polypyrrole composite for the treatment of real textile wastewater, J. Water Process Eng. 35 (2020), 101230.

[21] H. Liu, J. Zhang, M. Lu, L. Liang, H. Zhang, J. Wei, Biosynthesis based meEBrane filtration coupled with iron nanoparticles reduction process in removal of dyes, Chem. Eng. J. 387 (2020), 124202.

[22] P.B. Koli, K.H. Kapadnis, U.G. Deshpande, M.R. Patil, Fabrication and characterization of pure and modified Co3O4 nanocatalyst and their application for photocatalytic degradation of eosin blue dye: a comparative study, J. Nanostructure Chem. 8 (4) (2018) 453–463.

[23] S.E. Ebrahim, T.J. Mohammed, H.O. Oleiwi, Removal of acid blue dye from industrial wastewater by using reverse osmosis technology, Association of Arab Universities Journal of Engineering Sciences 25 (3) (2018) 29–40.

[24] Q. Long, Z. Zhang, G. Qi, Z. Wang, Y. Chen, Z.Q. Liu, Fabrication of chitosan nanofiltration meEBranes by the film casting strategy for effective removal of dyes/salts in textile wastewater, ACS Sustainable Chem. Eng. 8 (6) (2020) 2512–2522.

[25] P.V. Nidheesh, M. Zhou, M.A. Oturan, An overview on the removal of synthetic dyes from water by electrochemical advanced oxidation processes, Chemosphere 197 (2018) 210–227.

[26] S.G. Shinde, M.P. Patil, G.D. Kim, V.S. Shrivastava, Ni, C, N, S multi-doped ZrO2 decorated on multi-walled carbon nanotubes for effective solar induced degradation of anionic dye, J. Environ. Chem. Eng. 8 (3) (2020), 103769.

[27] P.B. Koli, K.H. Kapadnis, U.G. Deshpande, Transition metal decorated Ferrosoferric oxide (Fe3O4): An expeditious catalyst for photodegradation of Carbol Fuchsin in environmental remediation, J. Environ. Chem. Eng. 7 (5) (2019), 103373.

[28] M.R. Patil, S.D. Khairnar, V.S. Shrivastava, Synthesis, characterisation of polyaniline–Fe3O4 magnetic nanocomposite and its application for removal of an acid violet 19 dye, Appl. Nanosci. 6 (4) (2016) 495–502.

[29] J.J. Rueda-Marquez, I. Levchuk, P.F. Ibanez, M. Sillanpää, A critical review on application of photocatalysis for toxicity reduction of real wastewaters, J. Cleaner Prod. 258 (2020), 120694.

[30] A. Saravanan, P.S. Kumar, D.V.N. Vo, P.R. Yaashikaa, S. Karishma, S. Jeevanantham, B. Gayathri, V.D. Bharathi, Photocatalysis for removal of environmental pollutants and fuel production: a review, Environ. Chem. Lett. 19 (1) (2021) 441–463.

[31] S. Sharma, A. Umar, S.K. Mehta, A.O. Ibhadon, S.K. Kansal, Solar light driven photocatalytic degradation of levofloxacin using TiO 2/carbon-dot nanocomposites, New J. Chem. 42 (9) (2018) 7445–7456.

[32] N.K. Jangid, S. Jadoun, A. Yadav, M. Srivastava, N. Kaur, Polyaniline-TiO2-based photocatalysts for dyes degradation, Polym. Bull. 78 (8) (2021) 4743–4777.

[33] M.B. Tahir, S. Ali, M. Rizwan, A review on remediation of harmful dyes through visible light-driven WO3 photocatalytic nanomaterials, Int. J. Environ. Sci. Technol. 16 (8) (2019) 4975–4988.

[34] C. Parvathiraja, S. Shailajha, Bioproduction of CuO and Ag/CuO heterogeneous photocatalysis-photocatalytic dye degradation and biological activities, Appl. Nanosci. 11 (4) (2021) 1411–1425.

[35] K.K. Bera, M. Chakraborty, M. Mondal, S. Banik, S.K. Bhattacharya, Synthesis of α-β Bi2O3 heterojunction photocatalyst and evaluation of reaction mechanism for degradation of RhB dye under natural sunlight, Ceram. Int. 46 (6) (2020) 7667–7680.

[36] C. Sun, J. Yang, M. Xu, Y. Cui, W. Ren, J. Zhang, H. Zhao, B. Liang, Recent intensification strategies of SnO2-based photocatalysts: A review, Chem. Eng. J. 427 (2022), 131564.

[37] M. Nemiwal, T.C. Zhang, D. Kumar, Recent progress in g-C3N4, TiO2 and ZnO based photocatalysts for dye degradation: Strategies to improve photocatalytic activity, Sci. Total Environ. 767 (2021), 144896.

[38] R.H. Waghchaure, V.A. Adole, B.S. Jagdale, P.B. Koli, Fe3+ modified zinc oxide nanomaterial as an efficient, multifaceted material for photocatalytic degradation of MB dye and ethanol gas sensor as part of environmental rectification, Inorg. Chem. Commun. 140 (2022), 109450.

[39] M.A.M. Adnan, N.M. Julkapli, S.B. Abd Hamid, Review on ZnO hybrid photocatalyst: impact on photocatalytic activities of water pollutant degradation, Rev. Inorg. Chem. 36 (2) (2016) 77–104.

[40] R.H. Waghchaure, V.A. Adole, B.S. Jagdale, Photocatalytic degradation of methylene blue, rhodamine B, methyl orange and eriochrome black T dyes by modified ZnO nanocatalysts: a concise review, Inorg. Chem. Commun. (2022), 109764.

[41] S.G. Shinde, M.P. Patil, G.D. Kim, V.S. Shrivastava, Multi-doped ZnO photocatalyst for solar induced degradation of indigo carmine dye and as an antimicrobial agent, J. Inorg. Organomet. Polym Mater. 30 (4) (2020) 1141–1152.

[42] F. Luo, D. Zeng, W. Wang, Y. Yang, A. Zafar, Z. Wu, Y. Tian, Y. Huang, M. Hasan, X. Shu, Bio-conditioning poly-dihydromyricetin zinc nanoparticles synthesis for advanced catalytic degradation and microbial inhibition, J. Nanostructure Chem. (2021) 1–15.

[43] M.S. Saif, A. Zafar, M. Waqas, S.G. Hassan, A. ul Haq, T. Tariq, S. Batool, M. Dilshad, M. Hasan, X. Shu, Phyto-reflexive zinc oxide nano-flowers synthesis: an advanced photocatalytic degradation and infectious therapy, J. Mater. Res. Technol. 13 (2021) 2375–2391.

[44] M. Hasan, A. Zafar, I. Shahzadi, F. Luo, S.G. Hassan, T. Tariq, S. Zehra, T. Munawar, F. Iqbal, X. Shu, Fractionation of biomolecules in Withania coagulans extract for bioreductive nanoparticle synthesis, antifungal and biofilm activity, Molecules 25 (15) (2020) 3478.

[45] M. Hasan, M. Altaf, A. Zafar, S.G. Hassan, Z. Ali, G. Mustafa, T. Munawar, M.S. Saif, T. Tariq, F. Iqbal, M.W. Khan, Bioinspired synthesis of zinc oxide nano-flowers: A surface enhanced antibacterial and harvesting efficiency, Mater. Sci. Eng., C 119 (2021), 111280.

[46] T. Munawar, F. Mukhtar, M.S. Nadeem, S. Manzoor, M.N. Ashiq, K. Mahmood, S. Batool, M. Hasan, F. Iqbal, Fabrication of dual Z-scheme TiO2-WO3-CeO2 heterostructured nanocomposite with enhanced photocatalysis, antibacterial, and electrochemical performance, J. Alloy. Compd. 898 (2022), 162779.

[47] F. Mukhtar, T. Munawar, M.S. Nadeem, S.A. Khan, M. Koc, S. Batool, M. Hasan, F. Iqbal, Enhanced sunlight-absorption of Fe2O3 covered by PANI for the photodegradation of organic pollutants and antimicrobial inactivation, Adv. Powder Technol. 33 (8) (2022), 103708.

[48] T. Munawar, M.S. Nadeem, F. Mukhtar, M. Riaz, S. Batool, M. Hasan, F. Iqbal, Transition metal-doped SnO2 and graphene oxide (GO) supported nanocomposites as efficient photocatalysts and antibacterial agents, Environ. Sci. Pollut. Res. (2022) 1–22.

[49] M.S. Nadeem, T. Munawar, F. Mukhtar, S. Batool, M. Hasan, U.A. Akbar, A. S. Hakeem, F. Iqbal, Energy-levels well-matched direct Z-scheme ZnNiNdO/CdS heterojunction for elimination of diverse pollutants from wastewater and microbial disinfection, Environ. Sci. Pollut. Res. (2022) 1–18.

[50] R.A. Shinde, V.A. Adole, B.S. Jagdale, T.B. Pawar, Superfast synthesis, antibacterial and antifungal studies of halo-aryl and heterocyclic tagged 2, 3-dihydro-1H-inden-1-one candidates, Monatshefte für Chemie-Chemical Monthly 152 (6) (2021) 649–658.

[51] V.A. Adole, R.A. More, B.S. Jagdale, T.B. Pawar, S.S. Chobe, R.A. Shinde, S. L. Dhonnar, P.B. Koli, A.V. Patil, A.R. Bukane, R.N. Gacche, Microwave prompted solvent-free synthesis of new series of heterocyclic tagged 7-arylidene indanone hybrids and their computational, antifungal, antioxidant, and cytotoxicity study, Bioorg. Chem. 115 (2021), 105259.

[52] S.S. Pathade, V.A. Adole, B.S. Jagdale, PEG-400 mediated synthesis, computational, antibacterial and antifungal studies of fluorinated pyrazolines, Curr. Res. Green Sustainable Chem. 4 (2021), 100172.

[53] R.A. Shinde, V.A. Adole, B.S. Jagdale, B.S. Desale, Synthesis, antibacterial and computational studies of Halo Chalcone hybrids from 1-(2, 3-Dihydrobenzo [b][1, 4] dioxin-6-yl) ethan-1-one, J. Indian Chem. Soc. 98 (4) (2021), 100051.

[54] R.A. Shinde, V.A. Adole, B.S. Jagdale, Synthesis, Computational, Antibacterial and Antifungal Investigation of Two Tri-Fluorinated Chalcones of 1-(2, 3-Dihydrobenzo [b][1, 4] dioxin-6-yl) ethan-1-one, Polycyclic Aromat. Compd. (2021) 1–18.

[55] S.J. Rehm, A. Tice, Staphylococcus aureus: methicillin-susceptible S. aureus to methicillin-resistant S. aureus and vancomycin-resistant S. aureus, Clin. Infectious Diseases 51 (Supplement_2) (2010) S176–S182.

[56] J. Handzlik, A. Matys, K. Kieć-Kononowicz, Recent advances in multi-drug resistance (MDR) efflux pump inhibitors of Gram-positive bacteria S. aureus, Antibiotics 2 (1) (2013) 28–45.

[57] Y. Guo, G. Song, M. Sun, J. Wang, Y. Wang, Prevalence and therapies of antibiotic-resistance in Staphylococcus aureus, Front. Cell. Infect. Microbiol. 10 (2020) 107.

[58] R.S. Shinde, R.A. More, V.A. Adole, P.B. Koli, T.B. Pawar, B.S. Jagdale, B.S. Desale, Y.P. Sarnikar, Design, fabrication, antitubercular, antibacterial, antifungal and antioxidant study of silver doped ZnO and CuO nano candidates: a comparative pharmacological study, Curr. Res. Green Sustainable Chem. 4 (2021), 100138.

[59] J. Akhtar, M.B. Tahir, M. Sagir, H.S. Bamufleh, Improved photocatalytic performance of Gd and Nd co-doped ZnO nanorods for the degradation of methylene blue, Ceram. Int. 46 (8) (2020) 11955–11961.

[60] N.R. Khalid, A. Hammad, M.B. Tahir, M. Rafique, T. Iqbal, G. Nabi, M.K. Hussain, Enhanced photocatalytic activity of Al and Fe co-doped ZnO nanorods for eosin blue degradation, Ceram. Int. 45 (17) (2019) 21430–21435.
[61] S.M. Aydoghmish, S.A. Hassanzadeh-Tabrizi, A. Saffar-Teluri, Facile synthesis and investigation of NiO–ZnO–Ag nanocomposites as efficient photocatalysts for degradation of eosin blue dye, Ceram. Int. 45 (12) (2019) 14934–14942.
[62] S. Selvaraj, M.K. Mohan, M. Navaneethan, S. Ponnusamy, C. Muthamizhchelvan, Synthesis and photocatalytic activity of Gd doped ZnO nanoparticles for enhanced degradation of eosin blue under visible light, Mater. Sci. Semicond. Process. 103 (2019), 104622.